IIER - 767TH INTERNATIONAL CONFERENCE ON RECENT INNOVATIONS IN ENGINEERING AND TECHNOLOGY ICRIET, DOHA, QATAR, DECEMBER 10-11, 2019.

BIOMAGNETIC NANO-RHEO-PHARMACO-DYNAMIC TRANSPORT IN A STENOTIC ARTERY: *TARGETED DRUG DELIVERY SIMULATION*

*Ankita Dubey[1], B. Vasu[1], R.S.R.Gorla [2], M. Jawid[3] and O. Anwar Bég[3]**

[1]Department of Mathematics, Motilal Nehru National Institute of Technology Allahabad, Prayagraj, Uttar Pradesh- 211004, India.

[2]Department of Mechanical Engineering, Euclid Avenue, Cleveland State University, Ohio, USA.

[3]Multi-Physical/Bio-Fluid Mechanics Research, Department of Mechanical/Aeronautical Engineering, Salford University, Manchester, M54WT, UK.

Emails: rma1601@mnnit.ac.in; bvasu@mnnit.ac.in; r.gorla@yahoo.com; mohammadjawid@outlook.com; *O.A.Beg@Salford.ac.uk (Presenter)

1.INTRODUCTION

- Hemodynamics plays a critical role in the formation and evolution of cardiovascular diseases. Simulation of blood flow has been widely used in recent decades for better understanding the symptomatic spectrum of various diseases, in order to improve already existing treatments or to develop new therapeutic techniques. Blood vessels are tapered by the growth of atherosclerotic plaques that bulge into the lumen, resulting in *stenosed blood vessels*. When stenosis is developed in an artery, one of the most severe problems associated with this obstruction is the increased resistance and the concomitant reduction of the blood flow to the specific vascular bed supplied by the artery. Blood is suspension of various tiny particles in a continuous saline plasma solution. The plasma generally behaves as a Newtonian fluid whereas the whole blood (a suspension of cells and highly viscous in nature), exhibits the property of a non-Newtonian fluid, in particular in smaller vessels [1]. The non-Newtonian characteristics of blood emerge at low shear rate whereas at high shear rate blood usually behaves like a Newtonian fluid as observed in large arteries Magnetohydrodynamics (MHD) involves the motion of electrically-conducting fluids under the influence of an applied magnetic field. The presence of ions and iron in the haemoglobin molecule produces electrically-conducting properties in blood [2]. Streaming blood can therefore be manipulated via the application of extra-corporeal magnetic fields which may be static or alternating in nature. Arterial diseases such as arteriosclerosis may therefore be treated via biomagnetic therapy. Nanofluids display an enhancement in thermal conductivity, which is boosted with increasing volumetric fraction of nanoparticles as reported by Masuda *et al.* [3]. Nanoparticle doping has been implemented in many diverse technological sectors and is now being adopted in drug delivery (pharmacodynamics) and biomedical therapy. Blood also exhibits variation in viscosity with temperature and Vogel's model is commonly used in mathematical models. It has been shown clinically that injected nanoparticles help in improving the blood flow in diseased arteries, and when combined with magnetic properties this new field is known as magnetic targeted nano-drug therapy. Motivated by these developments, this presentation focuses on computational fluid dynamic (CFD) simulation of the nanoparticle drug delivery in *stenosed realistic hemodynamics* in small vessels (coronary arteries) where blood is considered as a viscoelastic second grade fluid with viscosity variation simulated as a function of temperature via the Vogel model. The Buongiorno model is employed for nanoscale (Brownian motion and thermophoresis) effects [4]. The finite element code FreeFEM++ [5] is utilized. Many interesting hemodynamic characteristics are visualized.

2. NON-DIMENSIONAL MATHEMATICAL MODEL

- A simplified two-dimensional mathematical model for blood flow in a real coronary artery is considered wherein blood flow is modelled as non-homogeneous fluid flow containing a suspension of nanoparticles. Blood rheology is simulated with the second grade Reiner-Rivlin fluid model. Both heat and mass transfer are included. For the simulation, the stationary case of the blood vessel is assumed i.e. the pulsatile nature of streaming blood is neglected. The velocity is taken as zero at the internal walls of the vessel which is modelled as a cylindrical tube in a cylindrical coordinate system (*r, ϕ, z*).

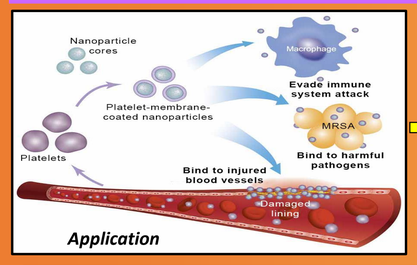

Application

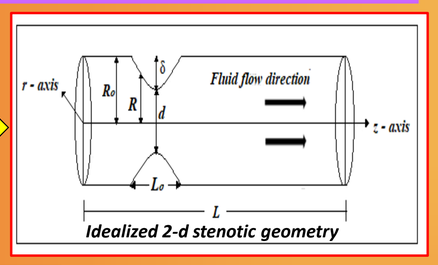

Idealized 2-d stenotic geometry

In the arterial segment the geometry of the mild stenosis is described by:

$$R(z) = \begin{cases} -R_0 + a\exp\left(-\frac{1}{2a^2}(z-\frac{L}{2}+0.5)^2\right); & L \le z \le L+L_0 \\ R_0 \quad ; & otherwise \end{cases}$$

Here the radius and length of the non-stenotic section are R_0, L_0 respectively and the radius of the stenotic part is taken as *R(z)*. The obstruction (stenosis) is symmetrical with a maximum height δ with $a = (5/4)\,\delta$ Neglecting the pressure gradient, the steady state, incompressible, two-dimensional non-dimensional governing equations for the nano-doped hydromagnetic blood transport are:

Primary momentum

Secondary momentum

Energy (heat)

Nano-particle concentration

$$\frac{cA}{SB^2}\frac{\partial\bar{\theta}}{\partial\bar{z}}\frac{\partial\bar{w}}{\partial\bar{r}} - \lambda_1\left[\frac{1}{\bar{r}}\left(\frac{\partial\bar{w}}{\partial\bar{r}}\right)^2 + 2\frac{\partial\bar{w}}{\partial\bar{r}}\frac{\partial^2\bar{w}}{\partial\bar{r}^2}\right] - \left(B_r\bar{\phi} + G_r\bar{\theta}\right) = 0$$

$$\frac{cA}{SB^2}\frac{\partial\bar{\theta}}{\partial\bar{r}}\frac{\partial\bar{w}}{\partial\bar{r}} - \lambda_1\left(\frac{\partial\bar{w}}{\partial\bar{z}}\frac{\partial^2\bar{w}}{\partial\bar{r}^2} + \bar{w}\frac{\partial^3\bar{w}}{\partial\bar{r}^2\partial\bar{z}} + \frac{\bar{w}}{\bar{r}}\frac{\partial^2\bar{w}}{\partial\bar{r}\partial\bar{z}} + \frac{1}{\bar{r}}\frac{\partial\bar{w}}{\partial\bar{r}}\frac{\partial\bar{w}}{\partial\bar{z}} + \frac{\partial\bar{w}}{\partial\bar{r}}\frac{\partial^2\bar{w}}{\partial\bar{r}\partial\bar{z}} + 2\frac{\partial\bar{w}}{\partial\bar{r}}\frac{\partial^2\bar{w}}{\partial\bar{z}\partial\bar{r}}\right) - \left(G_r\bar{\theta} + B_r\bar{\phi}\right) + M\bar{w} = 0$$

$$\left(\frac{\partial^2\bar{\theta}}{\partial\bar{r}^2} + \frac{1}{\bar{r}}\frac{\partial\bar{\theta}}{\partial\bar{r}}\right) + \left(N_b\left[\frac{\partial\bar{\phi}}{\partial\bar{r}}\frac{\partial\bar{\theta}}{\partial\bar{r}}\right] + N_t\left[\frac{\partial\bar{\theta}}{\partial\bar{r}}\frac{\partial\bar{\theta}}{\partial\bar{r}}\right]\right) = 0$$

$$\left(\frac{\partial^2\bar{\phi}}{\partial\bar{r}^2} + \frac{1}{\bar{r}}\frac{\partial\bar{\phi}}{\partial\bar{r}}\right) + \frac{N_t}{N_b}\left(\frac{\partial^2\bar{\theta}}{\partial\bar{r}^2} + \frac{1}{\bar{r}}\frac{\partial\bar{\theta}}{\partial\bar{r}}\right) = 0$$

non-dimensional boundary conditions

$$\bar{u} = 0,\ \bar{w} = 1,\ \frac{\partial\bar{w}}{\partial\bar{r}} = 0,\ \frac{\partial\bar{\theta}}{\partial\bar{r}} = 0,\ \frac{\partial\bar{\phi}}{\partial\bar{r}} = 0 \quad at\ \bar{r} = 0$$

$$\bar{u} = 0,\ \bar{w} = 0,\ \bar{\theta} = 1,\ \bar{\phi} = 1 \quad at\ \bar{r} = \bar{R}(z)$$

non-dimensional parameters

MHD i.e. magnetic body force parameter $M = \frac{\sigma B_0^2 L_0 R_0}{\mu_0}$, the Brownian motion parameter, $N_b = \frac{D_b(\phi_w - \phi_L)(\rho c)_p}{\kappa}$, thermophoresis parameter $N_t = \frac{D_T(\theta_w - \theta_L)(\rho c)_p}{\theta_L \kappa}$, the Grashof number $Gr = \frac{(\theta_w - \theta_L)\rho_{f,w} g(1-\phi_L)L_0 R_0 \beta_T}{U_0\mu_0}$, the Brownian diffusion constant $Br = \frac{(\rho_p - \rho_f)L_0 R_0(\phi_w - \phi_L)g}{U_0\mu_0}$, the Reynolds number $\mathrm{Re} = \frac{\rho_f U_0 L_0}{\mu_0}$, viscoelastic parameter $\lambda_1 = \frac{\alpha_1 U_0}{\mu_0 L_0}$, Prandtl number $\mathrm{Pr} = \frac{c_p\mu_0}{\kappa}$, and Schmidt number $S_c = \frac{\mu_0}{\rho_f D_b}$.

Non-dimensional skin friction coefficient

$$\frac{1}{2}C_f\,\mathrm{Re} = \frac{c}{S}\left[1 - \frac{A\bar{\theta}}{B^2}\right]\frac{\partial\bar{w}}{\partial\bar{r}} + \lambda_1\left(\bar{w}\frac{\partial^2\bar{w}}{\partial\bar{r}\,\partial\bar{z}} - \frac{\partial\bar{w}}{\partial\bar{r}}\frac{\partial\bar{w}}{\partial\bar{z}}\right)$$

Re is the local Reynolds number (which is the ratio of inertial to viscous forces)

3. FINITE ELEMENT SIMULATION WITH FREEFEM++

FreeFEM++ is an open source multi-physics programming software which allows fast and efficient solution of partial differential equations using the finite element method. This software offers several triangular finite elements, including discontinuous elements. It also provides options for simulating coupled electromagnetics, heat and mass diffusion and other phenomena. Using this method, the weak form of the governing Eqns. (*):

$$\int_\Omega \frac{cA}{SB^2}\frac{\partial\bar{\theta}}{\partial\bar{z}}\frac{\partial\bar{w}}{\partial\bar{r}}\cdot u\ dr - \int_\Omega \lambda_1\frac{1}{\bar{r}}\left(\frac{\partial\bar{w}}{\partial\bar{r}}\right)^2\cdot u\ dr - \int_\Omega 2\frac{\partial\bar{w}}{\partial\bar{r}}\frac{\partial^2\bar{w}}{\partial\bar{r}^2}\cdot u\ dr - \int_\Omega B_r\bar{\phi}\cdot u\ dr - \int_\Omega G_r\bar{\theta}\cdot u\ dr = 0$$

FREEFEM

$$\int_\Omega \frac{cA}{SB^2}\frac{\partial\bar{\theta}}{\partial\bar{r}}\frac{\partial\bar{w}}{\partial\bar{r}}\cdot v\ dr - \int_\Omega \lambda_1\frac{\partial\bar{w}}{\partial\bar{z}}\frac{\partial^2\bar{w}}{\partial\bar{r}^2}\cdot v\ dr - \int_\Omega \lambda_1\bar{w}\frac{\partial^3\bar{w}}{\partial\bar{r}^2\partial\bar{z}}\cdot v\ dr - \int_\Omega \lambda_1\frac{\bar{w}}{\bar{r}}\frac{\partial^2\bar{w}}{\partial\bar{r}\partial\bar{z}}\cdot v\ dr - \int_\Omega \lambda_1\frac{1}{\bar{r}}\frac{\partial\bar{w}}{\partial\bar{r}}\frac{\partial\bar{w}}{\partial\bar{z}}\cdot v\ dr - \int_\Omega \lambda_1\frac{\partial\bar{w}}{\partial\bar{r}}\frac{\partial^2\bar{w}}{\partial\bar{r}\partial\bar{z}}\cdot v\ dr - \int_\Omega 2\lambda_1\frac{\partial\bar{w}}{\partial\bar{r}}\frac{\partial^2\bar{w}}{\partial\bar{z}\partial\bar{r}}\cdot v\ dr - \int_\Omega G_r\bar{\theta}\cdot v\ dr - \int_\Omega B_r\bar{\phi}\cdot v\ dr + \int_\Omega M^2\bar{w}\cdot v\ dr = 0$$

$$\int_\Omega \frac{\partial^2\bar{\theta}}{\partial\bar{r}^2}\cdot w\ dr + \int_\Omega \frac{1}{\bar{r}}\frac{\partial\bar{\theta}}{\partial\bar{r}}\cdot w\ dr + \int_\Omega N_b\left[\frac{\partial\bar{\phi}}{\partial\bar{r}}\frac{\partial\bar{\theta}}{\partial\bar{r}}\right]\cdot w\ dr + \int_\Omega N_t\left[\frac{\partial\bar{\theta}}{\partial\bar{r}}\frac{\partial\bar{\theta}}{\partial\bar{r}}\right]\cdot w\ dr = 0$$

$$\int_\Omega \frac{\partial^2\bar{\phi}}{\partial\bar{r}^2}\cdot q\ dr + \int_\Omega \frac{1}{\bar{r}}\frac{\partial\bar{\phi}}{\partial\bar{r}}\cdot q\ dr + \int_\Omega \frac{N_t}{N_b}\left(\frac{\partial^2\bar{\theta}}{\partial\bar{r}^2} + \frac{1}{\bar{r}}\frac{\partial\bar{\theta}}{\partial\bar{r}}\right)\cdot q\ dr = 0$$

In the present study we consider classic Taylor-Hood triangular elements (P_1,P_2), 5928 unstructured fixed mesh elements with 12177 nodes as presented in Figure 2. The mesh is built taking advantage of an automatic FreeFEM++ [5] mesh generator based on the Delaunay-Voronoi algorithm. The non-linear system of the governing equations has been solved by employing the Generalized Minimal Residual (GMRES) iteration method. In the fixed mesh the prescribed minimum step size (h_{min}) is 0.0001 and the tolerance for computation is<10^{-6} for all simulations.

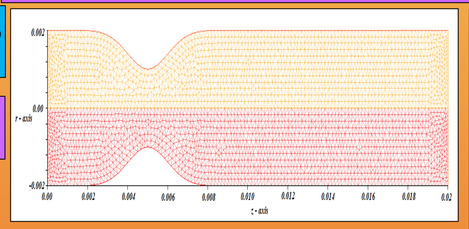

Unstructured fixed mesh of triangular elements

To ensure that the calculated numerical results are grid-independent, several different grid distributions have been tested. Table 1 shows the numerical values for velocity, temperature and nano-particle concentration for various designs of unstructured fixed mesh elements involving vertices and triangular elements as shown in Figure 2. Several different mesh distributions have been tested to ensure that the simulated numerical results are mesh independent. Therefore, the selected mesh for the present calculations consisted of 12177 nodes and 5928 triangular elements respectively. Increasing the mesh elements beyond this design does not modify significantly the numerical values of non-dimensional velocity, temperature, nano-particle concentration and skin-friction coefficient in the domain

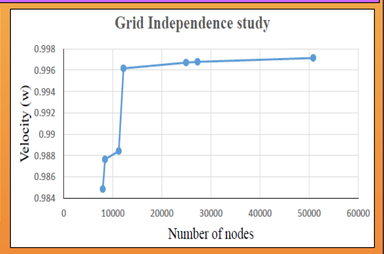

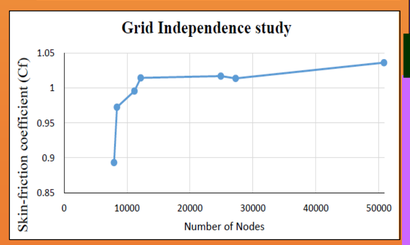

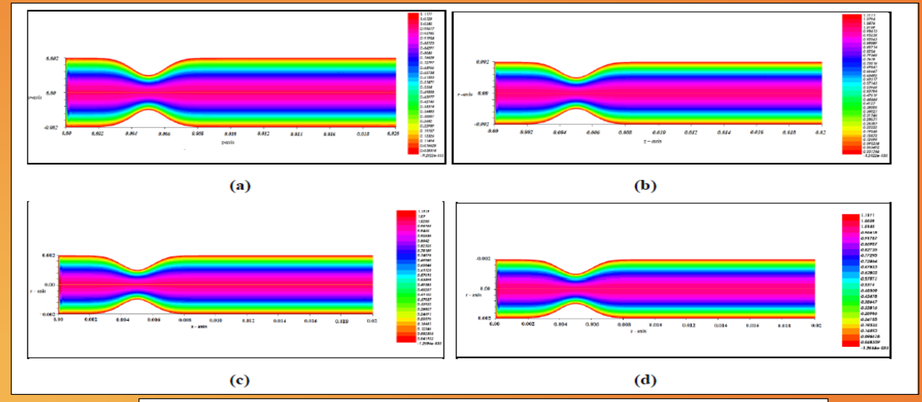

Figure Velocity field (a) $M = 0.3, N_b = 0.3$ *and* $N_t = 0.3$ *(b)* $M = 0.3, N_b = 0.3$ *and* $N_t = 0.6$, *(c)* $M = 0.6, N_b = 0.3$ *and* $N_t = 0.3$, *(d)* $M = 0.6, N_b = 0.3$ *and* $N_t = 0.6$.

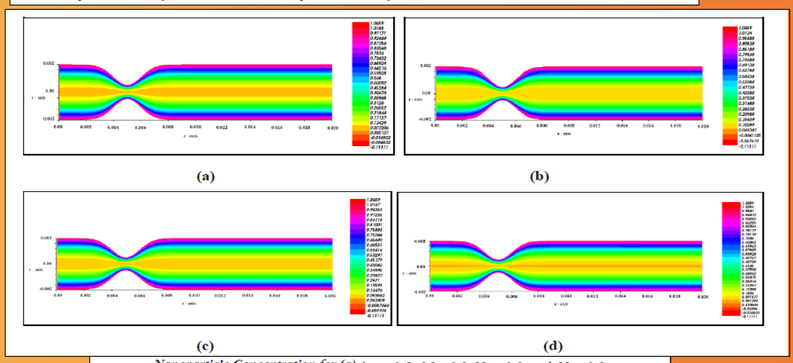

Nanoparticle Concentration for (a) $\lambda_1 = -0.5,\ M = 0.3, N_b = 0.3$ *and* $N_t = 0.3$, *(b)* $\lambda_1 = -0.5,\ M = 0.3, N_b = 0.3$ *and* $N_t = 0.6$, *(c)* $\lambda_1 = -0.5,\ M = 0.6, N_b = 0.3$ *and* $N_t = 0.3$ *(d)* $\lambda_1 = -0.5,\ M = 0.6, N_b = 0.3$ *and* $N_t = 0.6$.

5. DISCUSSION AND CONCLUSIONS

- Increasing the values of thermophoresis parameter, *Nt* from 0.3 to 0.6 (with magnetic parameter, *M*, and Brownian motion parameter, *Nb* fixed) decreases the value of velocity in whole domain. Thermophoresis relates to the migration of nano-particles under the force of a temperature gradient. With nano-particles migrating the momentum is inhibited in the arterial flow and deceleration induced. Effectively thermophoretic body force arises due to the averaged Brownian motion of particles in the nano-doped blood under a steady temperature gradient. Since steady state conditions are assumed, the stronger molecular impulses in the hotter nanofluid region mobilize nano-particles to migrate towards the colder region, where the molecular impulses are weaker. This destroys momentum in the blood flow and results in velocity decreasing. In particular, in the *core zone* strong deceleration is induced. With increasing magnetic parameter (*M*) there is also a significant decrement in velocity i.e. the core flow is again retarded. The presence of the Lorentzian magnetic drag force resists blood flow and especially generates deceleration in the constricted zone at the stenosis which in turn influences the remainder of the flow domain. In all plots, the velocity is maximum at centreline of the artery and decreases to the boundary at which it vanishes in accordance with the no-slip condition. Nano-particle contours show there is an expansion in the orange (lower magnitude contour) zone is expanded and the engulfing yellow zone (higher magnitude contour) is contracted. The values for nano-particle concentration are therefore reduced along the axial direction and radial direction in the vicinity of the stenotic region. Species diffusion of nano-particles into the core region is therefore decreased with greater thermophoretic effect. Comparing fig. a with fig. c, the magnetic parameter is increased from *M* = 0.3 to 0.6, with all other parameters fixed. A similar response to the thermophoretic effect is observed i.e. the orange zone is expanded and the yellow zone is diminished Stronger magnetic field therefore also inhibits nano-particle diffusion into the core zone and results in decreasing magnitudes of nano-particle concentration along the entire arterial section i.e. with all axial coordinate locations. Comparing fig. c and d this trend is further amplified with the emergence of a thin brown zone along the arterial mid-line indicating an even greater depletion in nano-particle concentration values. The combination of maximum magnetic parameter value and maximum thermophoresis parameter value therefore serves to strongly diminish nano-particle concentration values. The opposite effect i.e. *elevation in nano-particle diffusion* may therefore be induced by utilizing a weaker magnetic field and lower thermophoresis in nano-particle deployment in stenotic blood flows. Generally, no tangible modification in nano-particle concentration distribution at the vessel walls is induced with a change in either magnetic body force parameter or thermophoresis parameter. This is of potential relevance to clinical implementation in magnetic nano-drug delivery.

REFERENCES

[1] Ku D.N., Blood flow in arteries, *Ann. Rev. Fluid Mech.*, 29:399–434 (1997).

[2] Yousef Haik, Vinay Pai, and Ching-Jen Chen. Apparent viscosity of human blood in a high static magnetic field, *Journal of Magnetism and Magnetic Materials*, 225(1-2):180–186 (2001).

[3] H. Masuda *et al.* Alteration of thermal conductivity and viscosity of liquid by dispersing ultra-fine particles. Dispersion of Al2O3, SiO2 and TiO_2 ultra-fine particles, *Netsu Bussei*, 7, 227-233 (1993).

[4] J. Buongiorno, Convective transport in nanofluids. *ASME J. Heat Transfer,* 128, 3: 240-250 (2006).

[5] Mahmud K. R., Rhaman M. M. and Al Azad A. K., Numerical simulation and analysis of incompressible Newtonian fluid flows using FreeFem++, *Journal of Advanced Research in Fluid Mechanics and Thermal Sciences*, 26, 1-19 (2016).